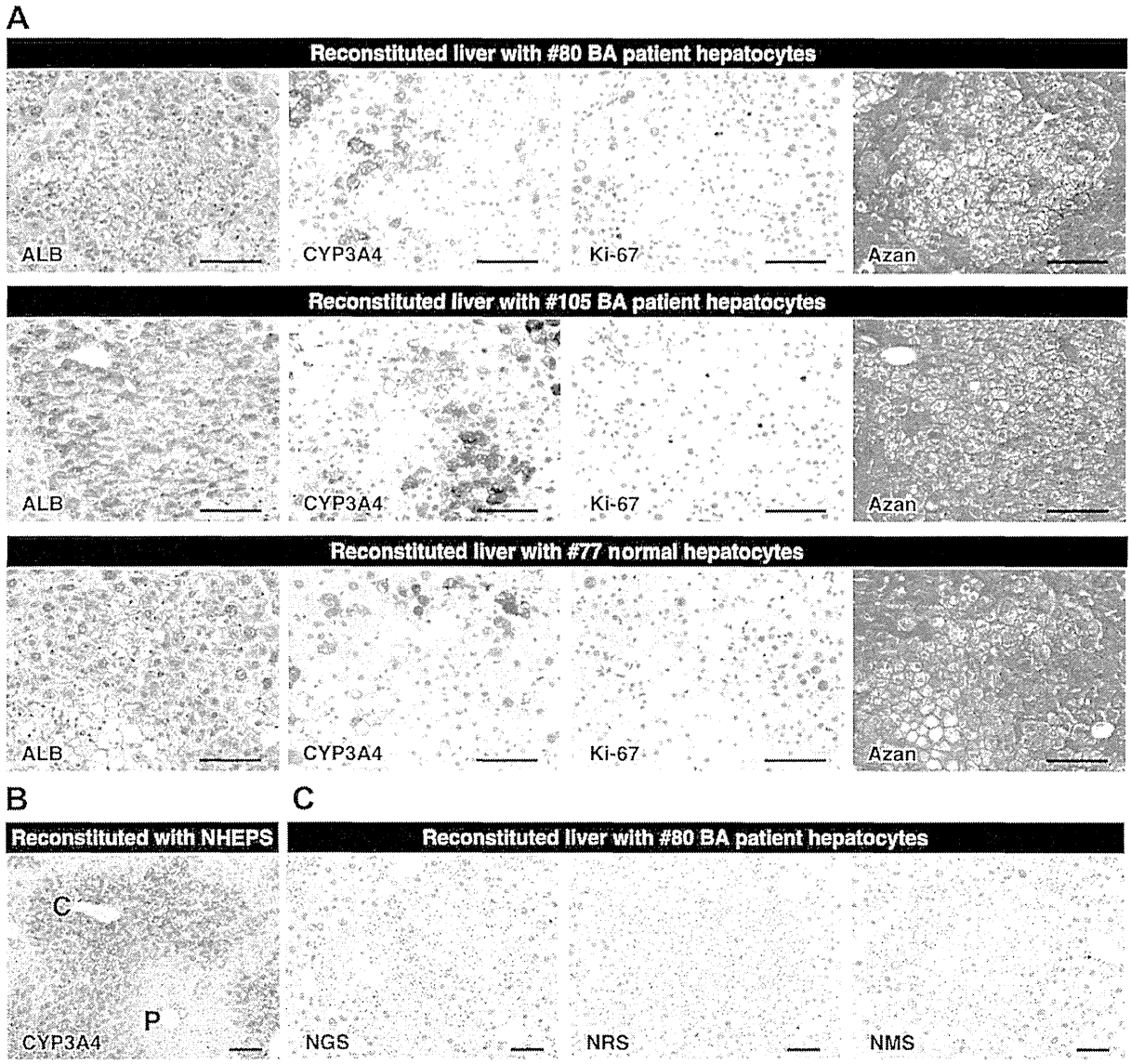

Figure 2. Immunohistochemistry of uPA-NOG mouse livers engrafted with BA patient hepatocytes. (A) Sections were stained for hALB, human CYP3A4, and human Ki-67 antigen; Azan-Mallory staining was also used. The scale bars represent 100 μm. (B) Immunohistochemical staining for CYP3A4 in a fully reconstituted uPA-NOG liver with NHEPS hepatocytes. The scale bar represents 100 μm. (C) Negative controls for immunostaining: NGS, NRS, and NMS. The scale bars represent 100 μm.

process was also observed in the colonies of NHEPS hepatocytes (Fig. 4, middle) but not in the HCT 116 colorectal tumors (Fig. 4, bottom). The typical BC network was detectable in the human hepatocyte conglomerates, as visualized by anti-MRP2, HLA antibodies, and H&E staining (Fig. 4). These results suggest that the intrahepatic bile duct system within the colonies reconstituted with hepatocytes from patients with BA must be nondefective.

DISCUSSION

BA is the most common reason for LT in children worldwide. The aim of this study was to evaluate regenerative medicine as a possible alternative to LT for treating BA. We succeeded in isolating viable hepatocytes from the livers of patients with BA so that we could evaluate the regenerative potential in vivo with a liver failure mouse model.[11] Recently, Gramignoli et al.[28] reported the successful isolation of hepatocytes from people with a number of different metabolic and other liver diseases (n = 35). The purpose of their study was to evaluate hepatocytes from individuals with metabolic disease for use in cell therapy via hepatocyte transplantation. Although they performed hepatocyte isolation in patients with BA (n = 7), those cells would not be recommended for clinical transplants because of concerns about cell yields, viability,

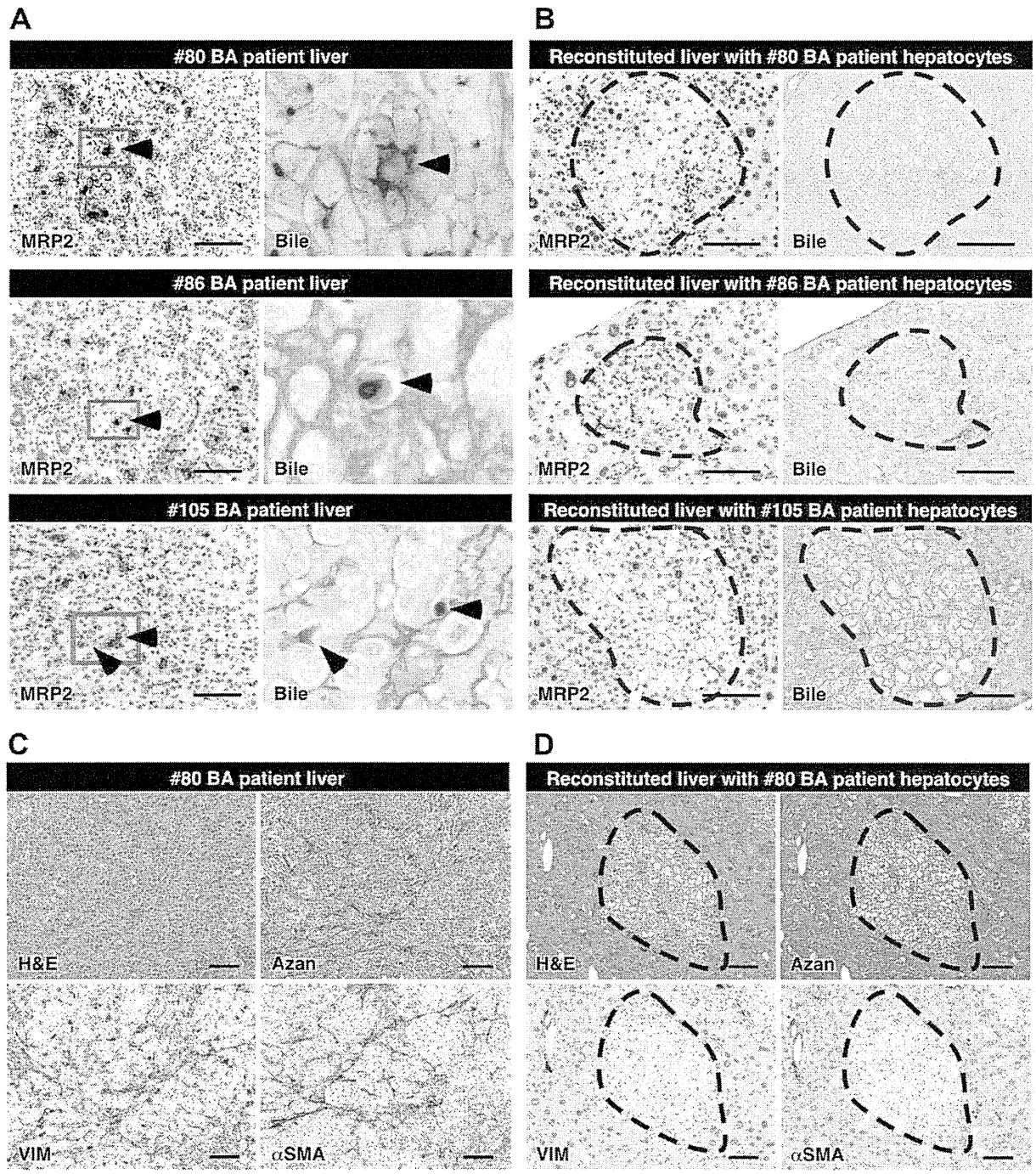

Figure 3. Detection of biliary obstructions and hepatic fibrosis. (A) Immunohistochemical staining for MRP2 protein in livers from patients with BA (patients 80, 86, and 105; left). Enlarged views of the boxed areas are shown with Hall's bilirubin staining (right). Bile stained with Hall's method appears green (arrowheads). (B) Immunohistochemical staining for MRP2 protein (left) and Hall's bilirubin staining (right) in uPA-NOG mouse livers engrafted with hepatocytes from BA patients (patients 80, 86, and 105). The dotted areas indicate the repopulated human liver. (C) H&E and Azan-Mallory staining and immunohistochemical staining for VIM and αSMA in the liver from a BA patient (patient 80). (D) H&E and Azan-Mallory staining and immunohistochemical staining for VIM and αSMA in a uPA-NOG mouse liver engrafted with hepatocytes from a BA patient (patient 80). The dotted areas indicate the repopulated human liver. The scale bars represent 100 μm.

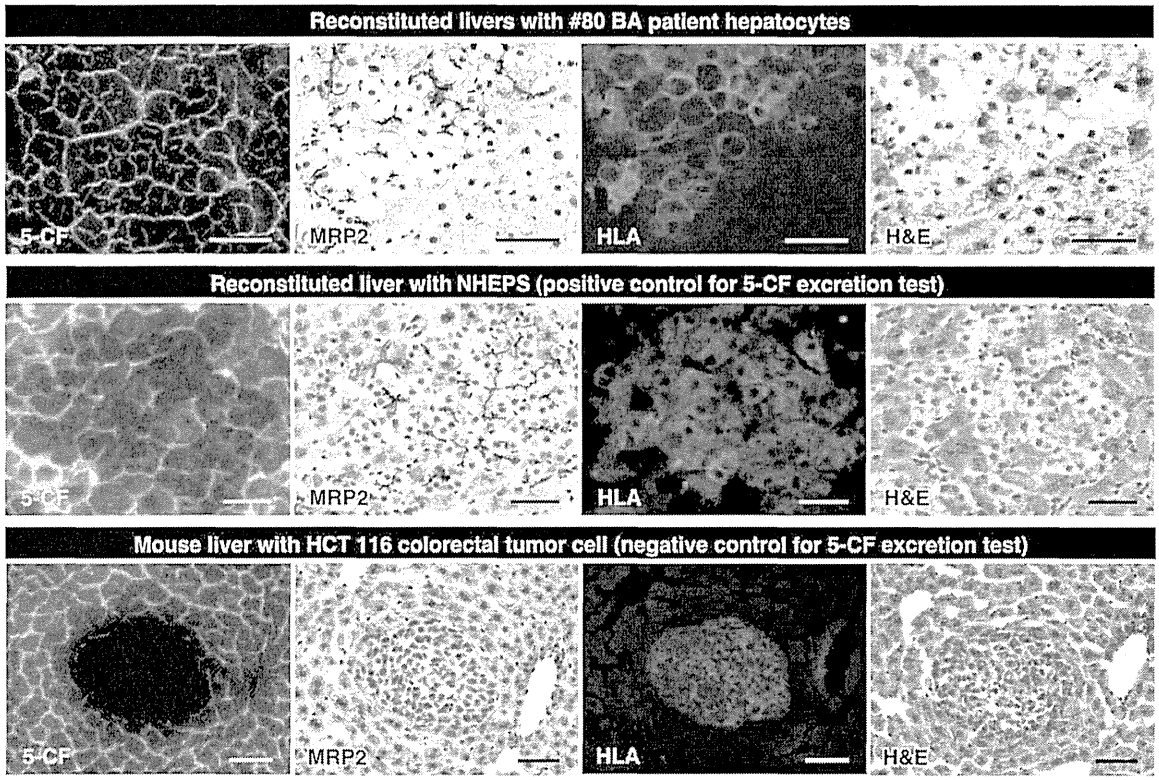

Figure 4. Functional integrity of the BC network within the reconstituted livers. Biliary excretion tests were performed with a fluorescent metabolic marker (5-CFDA). Serial sections were prepared from the livers of mice that received transplants of hepatocytes from a BA patient (patient 80), commercially available cryopreserved hepatocytes (NHEPS; positive control), or HCT 116 colorectal tumor cells (negative control). The sections were loaded with 5-CFDA, and the presence of the fluorescent metabolite 5-CF was assessed. In the livers reconstituted with patient hepatocytes and NHEPS hepatocytes, 5-CF (green on a dark field) was rapidly excreted into the BCs that formed the honeycomb networks over the lobule. In contrast, the BCs around the tumor, which formed after the transplantation of HCT 116 colorectal tumor cells, did not have this honeycomb pattern. Additional sections were stained for human MRP2 (brown in a bright field) and HLA (red in a dark field); H&E staining was also performed. The scale bars represent 50 μm.

and function. Bhogal et al.[29] reported that the viability, the total cell yield, and the success rate with cirrhotic tissues were low. In the current study, the cell yield and cell viability of hepatocytes from BA patients with fibrosis grade II or III were comparable to the yields and viability previously reported by Gramignoli et al. We expected that the low cell yield and viability would depend on the degree of fibrosis in patients with BA. However, there were no significant differences in the cell yields of hepatocytes from patients with grade II fibrosis and hepatocytes from patients with grade III fibrosis (Fig. 1C) or in cell viability (Fig. 1D). These results indicate that regardless of the extent of hepatic fibrosis, the presence of fibrosis affects the cell yield and viability when hepatocytes are isolated from the livers of patients with BA.

For hepatocytes from patient 80, 3 different conditions (freshly isolated, chilled, and frozen-thawed hepatocytes) were compared in terms of their engraftment and proliferative potential in a liver failure model using uPA-NOG mice. HLA-positive hepatocyte colonies were observed in the livers of all uPA-NOG mice that underwent transplantation with hepatocytes of any condition; however, a higher ratio of hALB-secreting mice and a higher level of serum hALB were observed in the mice that underwent transplantation with freshly isolated hepatocytes (Table 2). We succeeded in isolating a small number of hepatocytes buried in the severely cirrhotic liver of BA patient 149 (fibrosis grade III), and surprisingly, the hepatocytes could successfully engraft and proliferate within the uPA-NOG mouse livers as HLA-positive colonies. These results indicate that even hepatocytes buried in the cirrhotic livers of patients with BA do not lose their proliferative potential.

Recent studies of the molecular biology of BA have revealed no significant differences in the hepatic MRP2 expression levels of BA patients and control groups.[30] In fact, we confirmed the expression of not only the adenosine triphosphate–binding cassette, subfamily C (cystic fibrosis transmembrane conductance regulator (CFTR)/multidrug resistance-associated protein (MRP)), member 2 (ABCC2) gene but also the MRP2 protein, which was located on the apical plasma membranes of hepatocytes both in the livers of BA patients (Fig. 3A, left) and in partially humanized livers repopulated with hepatocytes from patients

with BA (Fig. 3B, left). Despite the normal MRP2 protein expression in the livers of patients with BA and in the partially humanized mouse liver, the bile was accumulated only in the many BCs of livers from patients with BA. This result clearly demonstrates the extrahepatic obstruction of the biliary flow.

In this study, using a reconstituted-liver mouse model, we examined the hepatocytes of patients with BA for the presence of abnormalities in vivo. Unfortunately, we failed to establish a BA model with liver-injured mice. However, this result indicates that the primary etiology of BA is absent in the hepatocytes themselves, and the hepatocytes buried in the cirrhotic livers of patients with BA are functionally intact hepatocytes retaining their proliferative potential and able to reconstitute a partially functioning human liver in mice. Gramignoli et al.[28] recently reported the isolation of hepatocytes from patients with many metabolic diseases, including BA, and the rapid and efficient repopulation of FRG (fumarylacetoacetate hydrolase (Fah), recombination activating gene 2 (Rag2) and interleukin 2 receptor gamma chain (Il-2rγ) triple gene knockout) mouse livers after the transplantation of hepatocytes obtained from patients with metabolic disease. In addition to Gramignoli et al.'s report, the current study supports the hypothesis that hepatocytes from patients with BA are morphologically and biochemically normal.

Recently, it has been reported that the extent of liver fibrosis at the time of portoenterostomy, as evaluated by picrosirius red staining, appears to be a strong negative predictor of outcomes.[31] The negative correlation between the extent of liver fibrosis and the yield of viable hepatocytes suggested by our results might be associated with that phenomenon. These results support the possibility that if the primary etiology is removed by Kasai portoenterostomy before progressive cholestasis develops, the liver of the patient with BA may regenerate autologously via the functionally intact hepatocytes remaining in the cirrhotic liver. The hepatocyte function in patients with BA may be independent of the degree of fibrosis; therefore, efforts to ameliorate the fibrosis would have great promise in treating this disease. Treatment would include an earlier diagnosis and surgery but might also include developing antifibrotic pharmacological approaches. If a method for earlier diagnosis or new drugs are developed in the near future, patients with BA may not require an operation that is as difficult as LT.

ACKNOWLEDGMENT

The authors thank M. Kuronuma, Y. Ando, T. Ogura, T. Kamisako, and R. Takahashi for their outstanding technical assistance with the animal experiments. They also thank M. Yamamoto, H. Nabekawa, and C. Kito for their technical assistance with molecular analyses and Dr. M. Ito, S. Enosawa, and M. Onodera for their helpful discussions.

REFERENCES

1. Hartley JL, Davenport M, Kelly DA. Biliary atresia. Lancet 2009;374:1704-1713.
2. Bassett MD, Murray KF. Biliary atresia: recent progress. J Clin Gastroenterol 2008;42:720-729.
3. Muratore CS, Harty MW, Papa EF, Tracy TF Jr. Dexamethasone alters the hepatic inflammatory cellular profile without changes in matrix degradation during liver repair following biliary decompression. J Surg Res 2009; 156:231-239.
4. Sokol RJ, Shepherd RW, Superina R, Bezerra JA, Robuck P, Hoofnagle JH. Screening and outcomes in biliary atresia: summary of a National Institutes of Health workshop. Hepatology 2007;46:566-581.
5. Serinet MO, Wildhaber BE, Broué P, Lachaux A, Sarles J, Jacquemin E, et al. Impact of age at Kasai operation on its results in late childhood and adolescence: a rational basis for biliary atresia screening. Pediatrics 2009;123: 1280-1286.
6. Czech-Schmidt G, Verhagen W, Szavay P, Leonhardt J, Petersen C. Immunological gap in the infectious animal model for biliary atresia. J Surg Res 2001;101:62-67.
7. Petersen C, Biermanns D, Kuske M, Schäkel K, Meyer-Junghänel L, Mildenberger H. New aspects in a murine model for extrahepatic biliary atresia. J Pediatr Surg 1997;32:1190-1195.
8. Riepenhoff-Talty M, Schaekel K, Clark HF, Mueller W, Uhnoo I, Rossi T, et al. Group A rotaviruses produce extrahepatic biliary obstruction in orally inoculated newborn mice. Pediatr Res 1993;33(pt 1):394-399.
9. Dandri M, Burda MR, Török E, Pollok JM, Iwanska A, Sommer G, et al. Repopulation of mouse liver with human hepatocytes and in vivo infection with hepatitis B virus. Hepatology 2001;33:981-988.
10. Mercer DF, Schiller DE, Elliott JF, Douglas DN, Hao C, Rinfret A, et al. Hepatitis C virus replication in mice with chimeric human livers. Nat Med 2001;7:927-933.
11. Suemizu H, Hasegawa M, Kawai K, Taniguchi K, Monnai M, Wakui M, et al. Establishment of a humanized model of liver using NOD/Shi-scid IL2Rgnull mice. Biochem Biophys Res Commun 2008;377:248-252.
12. Barshes NR, Lee TC, Udell IW, O'Mahoney CA, Karpen SJ, Carter BA, Goss JA. The Pediatric End-Stage Liver Disease (PELD) model as a predictor of survival benefit and posttransplant survival in pediatric liver transplant recipients. Liver Transpl 2006;12:475-480.
13. Weerasooriya VS, White FV, Shepherd RW. Hepatic fibrosis and survival in biliary atresia. J Pediatr 2004;144: 123-125.
14. Seglen PO. Preparation of isolated rat liver cells. Methods Cell Biol 1976;13:29-83.
15. Miyamoto Y, Suzuki S, Nomura K, Enosawa S. Improvement of hepatocyte viability after cryopreservation by supplementation of long-chain oligosaccharide in the freezing medium in rats and humans. Cell Transplant 2006;15:911-919.
16. Nakamura K, Mizutani R, Sanbe A, Enosawa S, Kasahara M, Nakagawa A, et al. Evaluation of drug toxicity with hepatocytes cultured in a micro-space cell culture system. J Biosci Bioeng 2011;111:78-84.
17. Hasegawa M, Kawai K, Mitsui T, Taniguchi K, Monnai M, Wakui M, et al. The reconstituted 'humanized liver' in TK-NOG mice is mature and functional. Biochem Biophys Res Commun 2011;405:405-410.
18. Tsukahara T, Kawaguchi S, Torigoe T, Asanuma H, Nakazawa E, Shimozawa K, et al. Prognostic significance of HLA class I expression in osteosarcoma defined by anti-pan HLA class I monoclonal antibody, EMR8-5. Cancer Sci 2006;97:1374-1380.

19. Key G, Becker MH, Baron B, Duchrow M, Schlüter C, Flad HD, Gerdes J. New Ki-67-equivalent murine monoclonal antibodies (MIB 1-3) generated against bacterially expressed parts of the Ki-67 cDNA containing three 62 base pair repetitive elements encoding for the Ki-67 epitope. Lab Invest 1993;68:629-636.
20. Scheffer GL, Kool M, Heijn M, de Haas M, Pijnenborg AC, Wijnholds J, et al. Specific detection of multidrug resistance proteins MRP1, MRP2, MRP3, MRP5, and MDR3 P-glycoprotein with a panel of monoclonal antibodies. Cancer Res 2000;60:5269-5277.
21. Dekel B, Shezen E, Even-Tov-Friedman S, Katchman H, Margalit R, Nagler A, Reisner Y. Transplantation of human hematopoietic stem cells into ischemic and growing kidneys suggests a role in vasculogenesis but not tubulogenesis. Stem Cells 2006;24:1185-1193.
22. Skalli O, Ropraz P, Trzeciak A, Benzonana G, Gillessen D, Gabbiani G. A monoclonal antibody against alpha-smooth muscle actin: a new probe for smooth muscle differentiation. J Cell Biol 1986;103(pt 2):2787-2796.
23. Hall MJ. A staining reaction for bilirubin in sections of tissue. Am J Clin Pathol 1960;34:313-316.
24. Hamada K, Monnai M, Kawai K, Nishime C, Kito C, Miyazaki N, et al. Liver metastasis models of colon cancer for evaluation of drug efficacy using NOD/Shi-scid IL2R-gammanull (NOG) mice. Int J Oncol 2008;32:153-159.
25. Limas C, Bigler A, Bair R, Bernhart P, Reddy P. Proliferative activity of urothelial neoplasms: comparison of BrdU incorporation, Ki67 expression, and nucleolar organiser regions. J Clin Pathol 1993;46:159-165.
26. Mills SJ, Shepherd NA, Hall PA, Hastings A, Mathers JC, Gunn A. Proliferative compartment deregulation in the non-neoplastic colonic epithelium of familial adenomatous polyposis. Gut 1995;36:391-394.
27. Kudo A, Kashiwagi S, Kajimura M, Yoshimura Y, Uchida K, Arii S, Suematsu M. Kupffer cells alter organic anion transport through multidrug resistance protein 2 in the post-cold ischemic rat liver. Hepatology 2004;39:1099-1109.
28. Gramignoli R, Tahan V, Dorko K, Skvorak KJ, Hansel MC, Zhao W, et al. New potential cell source for hepatocyte transplantation: discarded livers from metabolic disease liver transplants. Stem Cell Res 2013;11:563-573.
29. Bhogal RH, Hodson J, Bartlett DC, Weston CJ, Curbishley SM, Haughton E, et al. Isolation of primary human hepatocytes from normal and diseased liver tissue: a one hundred liver experience. PLoS One 2011;6:e18222.
30. Terui K, Saito T, Hishiki T, Sato Y, Mitsunaga T, Yoshida H. Hepatic expression of multidrug resistance protein 2 in biliary atresia. Comp Hepatol 2011;10:6.
31. Pape L, Olsson K, Petersen C, von Wasilewski R, Melter M. Prognostic value of computerized quantification of liver fibrosis in children with biliary atresia. Liver Transpl 2009;15:876-882.

Exp. Anim. 63(3), 321–330, 2014

—Original—

NOD-*Rag2*^{null} *IL-2Rγ*^{null} Mice: An Alternative to NOG Mice for Generation of Humanized Mice

Ikumi KATANO[1, 2], Ryoji ITO[1], Tsutomu KAMISAKO[1], Tomoo ETO[1], Tomoyuki OGURA[1], Kenji KAWAI[1], Hiroshi SUEMIZU[1], Takeshi TAKAHASHI[1], Yutaka KAWAKAMI[2], and Mamoru ITO[1]

[1]*Central Institute for Experimental Animals, 3-25-12 Tonomachi, Kawasaki-ku, Kawasaki, Kanagawa 216-0001, Japan*
[2]*Division of Cellular Signaling, Institute for Advanced Medical Research, Keio University School of Medicine, Shinjuku-ku, Tokyo 160-8582, Japan*

Abstract: We have developed NOD-*Rag2*^{null} *IL-2Rγ*^{null} (NR2G) mice similar to NOD-*scid IL-2Rγ*^{null} (NOG) mice that are known as an excellent host to generate humanized mice. To evaluate the usefulness of NR2G mice as a host for humanized mice, the engraftment rates and differentiation of human cells after human hematopoietic stem cell (HSC) transplantation were compared among NR2G, NOG, and NOD-*scid* mice. For this purpose, the appropriate irradiation doses to expand the niche for human stem cells in the bone marrow were first determined. As a result, 8 and 2.5 Gy in adult, and 4 and 1 Gy in newborn NR2G and NOG mice, respectively, were found to be appropriate. Next, 5×10^4 human umbilical cord blood CD34$^+$ cells were intravenously inoculated into irradiated adult or newborn of the immunodeficient mice. These HSC transplantation experiments demonstrated that both NR2G and NOG mice showed high engraftment rates compared with NOD-*scid* mice, although NOG mice showed a slightly higher engraftment rate than that for NR2G mice. However, no difference was found in the human cell populations differentiated from HSCs between NR2G and NOG mice. The HSC transplantation experiments to adults and newborns of two immunodeficient mice also revealed that the HSC transplantation into newborn mice resulted in higher engraftment rate than those into adults. These results showed that NR2G mice could be used as an alternative host to NOG mice to generate humanized mice.

Keywords: humanized mice, immunodeficient mice, NOD-*Rag2*^{null} *IL-2Rγ*^{null} mice, NOG mice

Introduction

Immunodeficient mice harboring human cells or tissues are considered useful for analyzing human biology *in vivo* without the ethical constraints associated with using humans themselves. These mouse models, termed humanized mice, would significantly advance our understanding of various human diseases and would facilitate development of new drugs against human diseases [18].

Recent advances in the development of newly immunodeficient mice such as NOD-*scid IL-2Rγ*^{null} (NOG/NSG) and BALB/c-*Rag2*^{null} *IL-2Rγ*^{null} (BR2G) mice have enabled the generation of humanized mice in which various human immune cells are successfully developed, and have promoted research in human biology and dis-

(Received 24 January 2014 / Accepted 18 March 2014)
Supplementary Figures: refer to J-STAGE: https://www.jstage.jst.go.jp/browse/expanim
Address corresponding: I. Katano, Central Institute for Experimental Animals, 3-25-12 Tonomachi, Kawasaki-ku, Kawasaki, Kanagawa 216-0001, Japan
Abbreviations: RAG2/1: recombination activating gene 2/1, HSC: hematopoietic stem cell, RBC: red blood cell, WBC: white blood cell, SPF: specific pathogen free, PB: peripheral blood, CB: umbilical cord blood, BM: bone marrow, SPL: spleen

eases [6, 14, 16]. Indeed, those studies not only showed an extremely high engraftment efficacy but also the development of multi-lineage human cells, including various subsets of T cells after transplantation of human umbilical cord blood (CB)-derived $CD34^+$ stem cells (HSCs) [4].

To generate appropriate humanized mice, the choice of immunodeficient mouse strains, human stem cell source, inoculation route, and mouse age used for cell transplantation are considered to be important. For a stem cell source, Lepus *et al.* [8] recently compared the engraftment and differentiation of human cells from various sources using three types of immunodeficient mice—NSG, BR2G, and C.B-17-*scid/bg* mice—and concluded that the use of $CD34^+$ stem cells from fetal liver and CB is suitable for studying human hematopoietic cell lineage development and function in humanized mice. However, the use of cells from aborted fetuses is not always feasible because of ethical issues in some countries. In this sense, the use of stem cells from CB may be more convenient for collection to circumvent ethical issues. For an inoculation route, intravenous inoculation has been used commonly for adult mice; by contrast, intrahepatic or intravenous inoculation has been used for newborn mice [4, 15]. However, it remains unresolved which route generates humanized mice more efficiently because of the different conditions, such as cell sources and mouse strains, used by researchers.

Regarding mouse strains, NOG/NSG and BRG mice are presently generally used for the generation of humanized mice. Pearson *et al.* [12] recently reported radioresistant NOD-*Rag1*^{null} *IL-2Rγ*^{null} (NR1G) mice, as well as NSG mice, showing high engraftment of human cells. Brehm *et al.* [2] compared the engraftment of human cells among NSG, NR1G, and BALB/c-*Rag1*^{null} *IL-2Rγ*^{null} (BR1G) mice generated based on *Rag1*^{null} mice and concluded that NSG and NR1G mice showed more efficient engraftment than BR1G mice. Both *Prkdc* and *Rag1/2* genes are responsible to compose T and B cell receptor genes resulting in T and B cell deficiency in mice mutated with both genes. SCID mice mutated with *Prkdc* gene but not with RAG1/2 genes have disadvantages in which irradiation sensitivity and T/B cell leakiness occurred [1, 3]. Therefore, Introduction of RAG1/2 mutation for *Prkdc*^{scid} mutation into mice may provide more stable immunodeficient strain of mice for xenotransplantation. We also independently developed NOD-*Rag2*^{null} *IL-2Rγ*^{null} (NR2G) mice based on *Rag2*^{null} mice. In the present study, we evaluated the usefulness of NR2G mice as humanized mice by comparing human cell engraftment and differentiation among NOG, NR2G, and NOD-*scid* mice after HSC transplantation.

Regarding mouse age, when HSCs are inoculated, adult or newborn mice have been used. Particularly, HSC inoculation into newborn mice is considered to be efficient because Traggiai *et al.* [16] reported humanized mice by HSC inoculation into newborn BRG mice. However, it is unclear what differences exist in the engraftment and differentiation of human cells from HSCs upon inoculation into newborn and adult mice. To address this issue, we compared the engraftment and differentiation of human cells in the mice when the same lot of CB $CD34^+$ cells was transplanted into newborn and adult NOG, NR2G, and NOD-*scid* mice.

Materials and Methods

Mice

NOD.CB17-*Prkdc*^{scid}/ShiJic (NOD-*scid*), NOD.Cg-*Prkdc*^{scid} *Il2rg*^{tm1Sug}/Jic (NOD-*scid IL-2Rγ*^{null}: NOG), NOD.Cg-*Rag2*^{tm1Fwa} *Il2rg*^{tm1Sug}/ShiJic (NOD-*Rag2*^{null} *IL-2Rγ*^{null}: NR2G, here termed to distinguish from NR1G of NOD-*Rag1*^{null} *IL-2Rγ*^{null} mice), and BALB/c-*Rag2*^{null} *IL-2Rγ*^{null} (BR2G) were used in the present study. NOD-*scid* mice were purchased from CLEA Japan, Inc. (Tokyo, Japan). NOG and NR2G mice were maintained at the Central Institute for Experimental Animals (CIEA). NR2G mice, first described in the present study, were generated as follows. NOD.Cg-*Rag2*^{tm1Fwa}/Jic mice were generated by the six-generation backcross-mating of B6.129S1-*Rag2*^{tm1Fwa}/JJic mice [13], which were originally a gift from Dr. Alt F. of Columbia University, into NOD mice using a speed congenic technique combining a marker-assisted selection protocol and *in vitro* fertilization [15]. NR2G mice were obtained by intercross mating among the offspring (NOD-*Rag2*$^{+/-}$ *IL-2Rγ*$^{+/-}$) between NOD-*Rag2*^{null} and NOD-*IL-2Rγ*^{null} mice.

For HSC transplantation experiments, adult mice were obtained by natural mating, and newborn mice were obtained by Cesarean section from recipient IQI females transplanted with NR2G embryos into the oviduct after *in vitro* fertilization. The newborn mice were nursed by IQI foster mothers until weaning after irradiation and cell transplantation.

The present study was performed in accordance with institutional guidelines and was approved by the Animal Experimentation Committee of CIEA.

Irradiation

Adults and newborns of NOG, NR2G, and BR2G mice were irradiated with 0–12 Gy using an X-ray irradiation device (MBR-1505R; Hitachi Medical Co., Tokyo, Japan) to determine an appropriate dose for the respective mice. The body weight of NOG, NR2G, and BR2G mice was measured each week for 4 or 8 weeks after irradiation using a scale (Pocket Scale 80; BOMSO, Tokyo, Japan).

Transplantation of human HSCs

The same lot of commercially available human CB derived $CD34^+$ cells (Lonza, Basel, Switzerland) was used in the current study. The frozen cells were incubated for a few minutes in a 37°C water bath, and then were moved quickly into phosphate-buffered saline (PBS) containing 2% fetal bovine serum. After washing with PBS, the viability of $CD34^+$ cells was examined by dye exclusion using 2.5% Trypan blue solution, and the cells with more than 80% viability were used for transplantation into the mice. For HSC transplantation into adult mice at 8 to 9 weeks of age, 5×10^4 of $CD34^+$ cells were inoculated intravenously via the tail vein at 24 h after irradiation. Newborn mice were irradiated at a day after birth, and 5×10^4 $CD34^+$ cells were inoculated intravenously via the facial vein at 24 h after irradiation.

Flow cytometry

To identify human cells in mouse peripheral blood (PB), the spleen, and the bone marrow (BM), multicolor flow cytometric analysis was performed using a FACSCanto flow cytometer (Becton Dickinson, Franklin Lakes, NJ, USA) with FACS Diva software (ver. 5.0.2; Becton Dickinson).

PB was collected periodically from the retro-orbital venous plexus using a capillary pipette (Drummond Scientific, Broomall, PA, USA) coated with heparin (Novo-Heparin 5000 units for Injection; Mochida Pharmaceutical Co., Tokyo, Japan) under anesthesia with isoflurane between 8 and 20 weeks after transplantation.

Mice were sacrificed by exsanguinating under anesthesia between 22 and 23 weeks after HSC transplantation. PB was collected from an abdominal vein, and the femurs, spleens and thymuses were also removed. After preparation of single cell suspensions and following treatment with red blood cell (RBC) lysis solution (0.154 M NH_4Cl, 13.770 mM $NaHCO_3$, 0.102 mM EDTA-2Na) to eliminate RBCs, white blood cells (WBCs) were suspended in PBS containing 2% fetal bovine serum. The cells were incubated with human-specific antibodies for 30 min at 4°C under protection from light.

The anti-human antibodies used for staining were fluorescein isothiocyanate (FITC)-conjugated anti-human CD45 (clone HI30; Becton Dickinson), anti-human CD33 (clone HIM3-4; BD Pharmingen, Franklin Lakes, NJ, USA), and anti-human CD4 (clone RPA-T4; eBioscience, Inc., San Diego, CA, USA); phycoerythrin (PE)-conjugated anti-human CD3 (clone UCHT1 555333; BD Pharmingen), PE-Cy7-conjugated anti-human CD3 (clone UCHT1; Beckman Coulter, Brea, CA, USA), and anti-human CD19 (clone J4.119; Beckman Coulter); allophycocyanin (APC)-conjugated anti-human CD8a antibody (clone OKT8; eBioscience, Inc.), anti-mouse CD45 antibody (clone 30-F11; BD Pharmingen), and APC-Cy7-conjugated anti-human CD45 (clone 2D1; BD Pharmingen). The engraftment rate of human cells was expressed as a percentage of human $CD45^+$ cells in the total human $CD45^+$ and mouse $CD45^+$ cells. The ratio of human immune cells was expressed as a percentage of human $CD3^+$, $CD19^+$, $CD4^+$, and $CD8^+$ cells in human $CD45^+$ cells.

Immunochemistry

To identify human cells in the spleen of transplanted mice, the spleens were removed from the mice after blood removal, and tissues were fixed with 10 nM formalin (10 nM Mildform; Wako, Tokyo, Japan), embedded in paraffin, and stained with hematoxylin and eosin (HE), mouse anti-human CD45 antigen monoclonal antibody (clone 2B11+PD7/26; Dako Cytomation, Glostrup, Denmark), rabbit anti-human CD3 monoclonal antibody (clone SP7; Nichirei, Tokyo, Japan), and mouse anti-human CD79a monoclonal antibody (clone JCB117; Nichirei). Briefly, 5-μm-thick sections of femurs and spleens on amino-silane coated glass slides (Matsunami glass, Osaka, Japan) were immunostained by the universal immuno-enzyme polymer method (Nichirei). Each of the anti-human antibodies was incubated overnight at 4°C. Sections were serially incubated with peroxidase-labeled polymer-conjugated goat anti-mouse antibody (Histofine Simplestain Max-PO; Nichirei) for 30 min at room temperature. Immunoreaction products were visualized by incubation with 0.02% 3, 3'-diaminobenzidine (DBA; Dojindo, Kumamoto, Japan) containing 0.006% H_2O_2. Immunostained sections were counterstained with hematoxylin for visualization of nuclei.

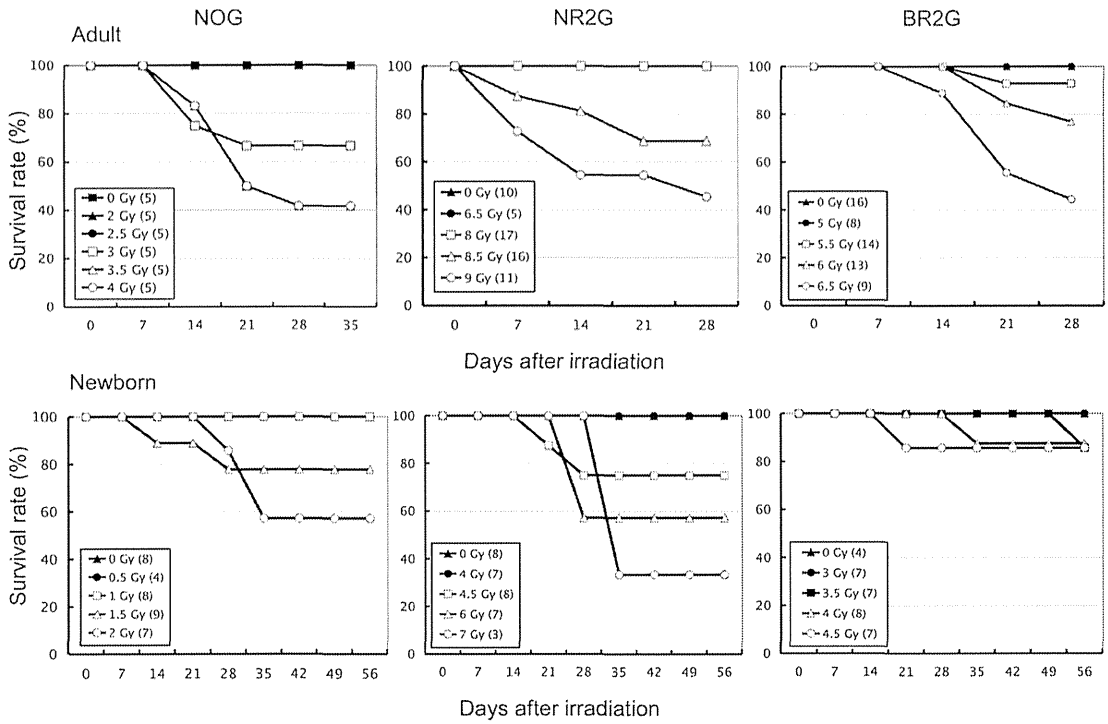

Fig. 1. Sensitivity of immunodeficient mice to total-body irradiation. Adult and newborn NOG, NR2G, and BR2G mice were irradiated with 0–12 Gy using an X-ray irradiation device to determine the appropriate dose. The body weight of NOG, NR2G, and BR2G mice was measured every week beginning 4 or 8 weeks after irradiation using a scale.

Statistical analysis

Mean values and standard deviations were calculated using the Excel software (Microsoft, Redmond, WA, USA). Significant differences were identified using Student's *t*-test, and a *P*-value less than 0.05 was deemed to indicate statistical significance.

Results

Radiation sensitivity of immunodeficient mice

Prior to transplantation experiments of human HSCs, the radiation sensitivity of adult and newborn mice of NOG, NR2G, and BR2G mice was investigated to determine an appropriate irradiation dose for HSC transplantation in each mouse strain. After irradiation into the mice with a dose ranging from 0.5 to 12 Gy, the body weight was periodically measured, and general observation was also performed for 26 days in adults and 56 days in newborns after irradiation, respectively. Non-irradiated mice in each strain were used as controls. As shown in Fig. 1, the minimum irradiation doses for the survival of all mice of each strain were 2.5 Gy, 8 Gy, and 5.5 Gy in adults, and 1 Gy, 4 Gy, and 3.5 Gy in newborns of NOG, NR2G, and BR2G mice, respectively. Thus extremely high resistance to irradiation was observed in NR2G mice.

Engraftment of human cells after HSC transplantation into adults and newborns of immunodeficient mice

The engraftment and differentiation of human cells were investigated when HSCs were transplanted into adult or newborn NOG, NR2G, and NOD-*scid* mice using the experimental protocol shown in Table 1. The 2.5-Gy dose of irradiation for adult NOD-*scid* mice used here was described previously [17], and this dose was equivalent with that of adult NOG mice. Therefore, the 1-Gy dose for newborn NOG mice was used for newborn NOD-*scid* mice.

Table 2 summarizes the engraftment rates of human cells into the adults and newborns of three strains of mice at 20 weeks after HSC transplantation. Twenty weeks after cell transplantation into NOG mice, 3 (30%) of 10 adult mice died, but none of the six newborn mice died during the same period. By contrast, all of the trans-

Table 1. Experimental conditions for human cell engraftment in immunodeficient mice

Mouse strain	Age for injection	No. of mice	Dose of irradiation (Gy)	Route of injection
NOG	Adult	10	2.5	Tail vein
	Newborn	6	1	Facial vein
NR2G	Adult	10	8	Tail vein
	Newborn	6	4	Facial vein
NOD-*scid*	Adult	9	2.5	Tail vein
	Newborn	5	1	Facial vein

Table 2. Human cell engraftment in adults or newborns of three strains of immunodeficient mice at 20 weeks after $CD34^+$ cell transfer

Age for injection	Mouse strain	No. of mice	Survival rate (%)	Frequency of engrafted mice (%)	Human $CD45^+$ cells (%)*
Adult	NOG	10	70 (7/10)	100 (7/7)	50.8 ± 17.2
	NR2G	10	100 (10/10)	100 (10/10)	40.0 ± 12.4
	NOD-*scid*	9	55.6 (5/9)	100 (5/5)	43.4 ± 14.6
Newborn	NOG	6	100 (6/6)	100 (6/6)	69.9 ± 4.5
	NR2G	6	83.3 (5/6)	100 (5/5)	43.1 ± 9.9
	NOD-*scid*	5	40 (2/5)	100 (2/2)	12.3 ± 2.1

*Percentages of human $CD45^+$ cells in mononuclaer cells of peripheral blood.

planted adult NR2G mice survived, but 1 (17%) of 6 newborn mice died. Human cells could be engrafted successfully in all surviving mice. When the engraftment rate of human cells was compared among the three strains of the mice, no significant difference was observed among adult mice of the three mouse strains. However, a significant difference was noted among the mouse strains when human cells were transplanted into newborn mice—namely, engraftment was higher in NOG, NR2G, and NOD-*scid* mice, in that order.

To examine the time course of human cell engraftment and differentiation from HSCs, the peripheral blood of the transplanted mice were collected at 8, 12, 16, and 20 weeks after HSC transplantation into adults and newborns mice, and then were analyzed by flow cytometry (Figs. 2 and 3).

In NOG and NR2G mice, only $CD19^+$ B cells were detected at 8 weeks after HSC transplantation. $CD3^+$ T cells were detected at 12 weeks after transplantation and reached 20% at 16 weeks in the NOG and NR2G mice. By contrast, only $CD19^+$ B cells, not $CD3^+$ T cells, developed during all periods tested in NOD-*scid* mice. The same results were obtained in transplanted adult and newborn mice, suggesting no significant difference in the differentiation of human cells. Conversely, engraftment of human cells was higher in transplanted NOG mice than in transplanted NR2G mice for both newborns and adults.

Human cells in the BM, the spleen, and PB of HSC transplanted mice

The human cell engraftment rates in the BM, the spleen, and PB at 22–23 weeks after cell transplantation into adult and newborn mice are shown in Supplemental Data Fig. 1. Extremely high engraftment rates were observed in both NOG and NR2G mice regardless of the transplanted age of the mice. Human cell engraftment rates were higher in the spleen, the BM, and PB, in that order, and this tendency was identified regardless of the transplanted age of the mice. The transplanted newborn mice showed higher engraftment rates than transplanted adult mice. However, no difference in the engraftment rate was observed between NOG and NR2G mice, except in PB from the newborn transplanted mice. The percentage of T, B cells and other lineage cells in human $CD45^+$ cells of the BM, the spleen, and PB are shown in Fig. 4. $CD3^+$ T cells were dominant in PB, but $CD19^+$ B cells were dominant in the BM and spleen of both NOG and NR2G mice. Particularly, a few $CD3^+$ cells were detected in the BM. No difference in the T- and B-cell subsets was noted in transplanted adult and newborn mice. For other lineage cells including NK cells and

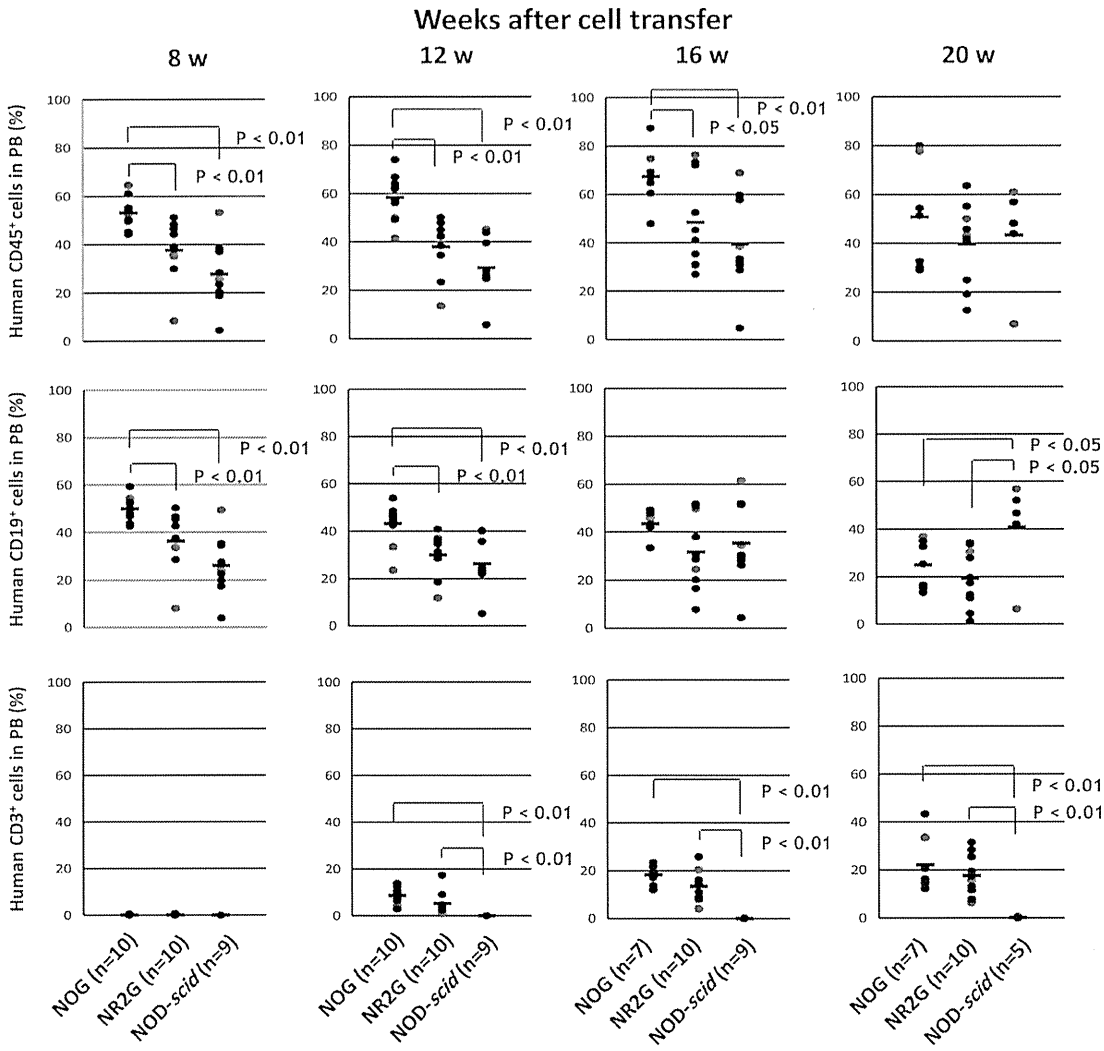

Fig. 2. Human cells in mouse peripheral blood after HSC transplantation into adult immunodeficient mice. A total of 5×10^4 commercially available human CB $CD34^+$ cells was intravenously inoculated via the tail vein in adult mice at 24 h after irradiation. After HSC transplantation, PB was collected periodically from the retro-orbital venous plexus using a capillary pipette coated with heparin under anesthesia with isoflurane at 8–20 weeks after transplantation. Human cells in mouse PB were analyzed by flow cytometry.

myeloid cells, only a small numbers of them were observed in NOG and NR2G mice, and there was also no difference among them (Data not shown).

T-cell subsets in PB, the spleen, and the thymus from HSC transplanted mice

To investigate the differentiation potential of T cell subsets, human $CD3^+$, $CD4^+$, and $CD8^+$ cells were examined in the BM, spleen, and thymus of both strains of mice. The ratios of $CD4^+$ cells were twofold those of $CD8^+$ cells in all organs tested. In the thymus, $CD4^+CD8^+$ T cells were dominant, as in humans. Here, no difference in the ratios of these T-cell subsets was observed in all organs of both mouse strains (Table 3). In addition, no difference in T-cell subset differentiation was observed between the adult and newborn transplanted mice. These results indicate that T-cell subsets can develop from HSCs in both strains, regardless of the transplanted age.

Distribution of human cells in the spleen

To investigate the distribution of human cells in the spleens of NOG and NR2G mice, we performed im-

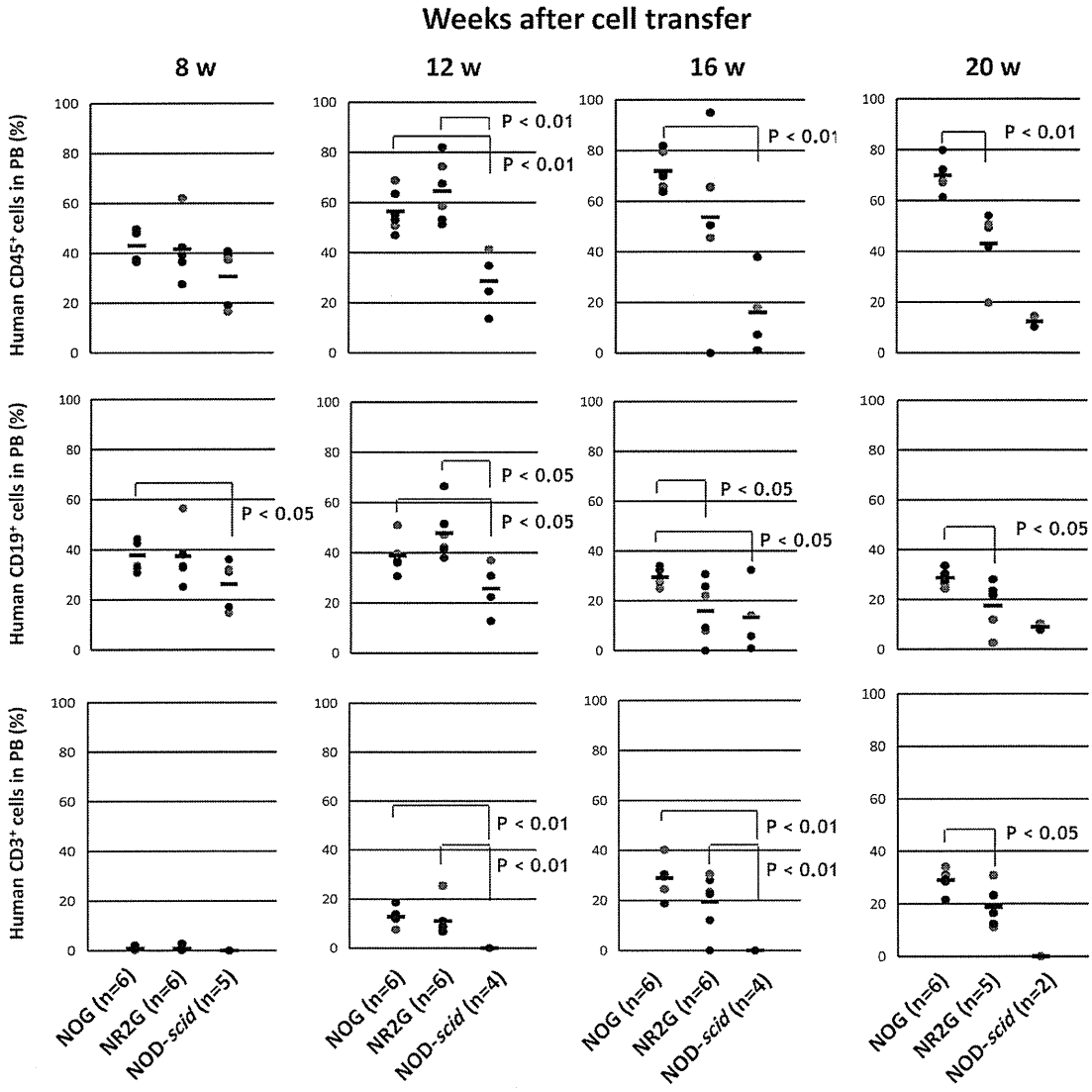

Fig. 3. Human cells in mouse peripheral blood after HSC transplantation into newborn immunodeficient mice. A total of 5×10^4 commercially available human CB $CD34^+$ cells was intravenously inoculated via the facial vein in newborn mice at 24 h after irradiation. After HSC transplantation, the analysis was done in the same manner as described in Figure 2. The number of NOD-*scid* mice (n=2) at 20 weeks after HSC transplantation was so small for statistical analysis that the mice were excluded in statistical analysis.

munohistological staining of the spleen using anti-human CD45, CD79a, and CD3 antibodies. As shown in Supplemental Data Fig. 2, human $CD45^+$ cells were broadly distributed in the spleen and formed strongly concentrated round-shaped areas. In these areas, $CD79a^+$ B cells were located in the periphery, whereas $CD3^+$ T cells were found in the central regions. Such structures were also observed in NOG and NR2G mice regardless of their transplanted age.

Discussion

In the present study, we established NR2G mice by introducing the *Rag2*^{null} gene into NOD-*IL-2Rγ*^{null} mice and investigated the capacity of the NR2G mice as recipients for human cell development after HSC transplantation in comparison to NOG mice, which are currently used extensively for generating humanized mice. In addition, we investigated the differences in human cell development and differentiation when HSCs are

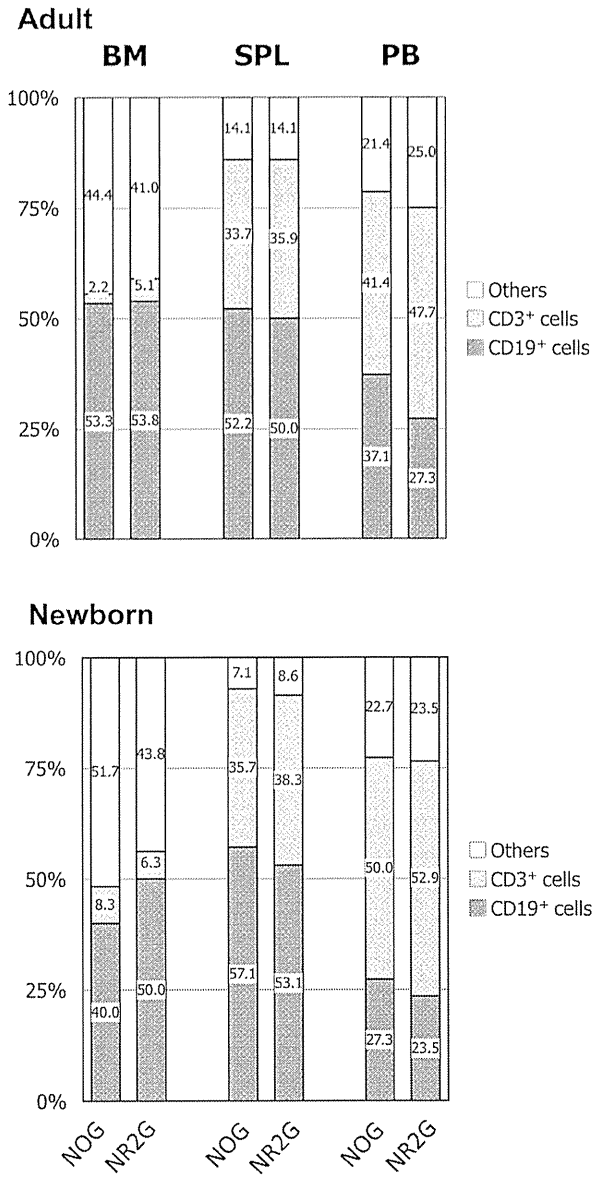

Fig. 4. Human T and B cells in the BM, spleen and PB of HSC-transplanted mice at 20 weeks after HSC transplantation. Figures in the column represent the percentage of each cell type among human CD45$^+$ cells. The number of NOG and NR2G mice used in this figure was 7 and 10 in adult, and 6 and 5 in newborn, respectively.

transplanted into newborns and adults of these immunodeficient mice.

Prior to HSC transplantation, irradiation sensitivities were determined in NOG, NR2G, and BR2G mice. NR2G mice showed high resistance against irradiation, similar to that in NR1G mice reported by Pearson *et al.* [12], compared with NOG and NOD-*scid* mice with the *Prkdc*^{scid} gene in which DNA double-strand break repair is impaired [3]. However, the irradiation resistance of NR2G mice was higher than that of NR1G mice. Namely, all NR2G mice survived for at least 26 days after 8-Gy irradiation to adult mice and at least 56 days after 4-Gy irradiation to newborn mice. By contrast, 30% of NR1G adult mice died within 28 days after 7-Gy irradiation. The reason for this difference in irradiation resistance between the NR2G and NR1G mice remains unclear. The difference between the targeted *Rag2* and *Rag1* genes in both mouse types is unlikely to affect irradiation resistance because both genes are closely located on chromosome 2 [10], and the targeting strategy and resulting phenotypes are quite similar between them [9, 13]. One explanation may be the difference in the irradiation source, namely X-ray irradiation for NR2G mice and ^{137}Cs irradiation for NR1G mice. Another explanation may be the difference in environmental factors, including the intestinal flora. Ivanov *et al.* [7] reported that the intestinal flora influenced the appearance of T helper cells in the intestinal lymphoid apparatus and demonstrated that the responses differed among mice with different flora from different breeders. The difference in the irradiation resistance between the mouse strains may be due to differences in the intestinal flora because damage to the intestine—in which cell turnover is rapid—causes early death after irradiation. Differences in irradiation sensitivity among mouse strains have been reported [11]; however, these differences are not likely to exist between NOD/LtSz and NOD/ShiJic mice because they are closely related in genetics as substrains.

Table 3. Percentages of T-cell subsets in the spleen, thymus, and peripheral blood of HSC-transplanted mice

Age in injection	Mouse strain	No. of mice	Spleen			Peripheral blood			Thymus			
			hCD3	hCD4	hCD8	hCD3	hCD4	hCD8	hCD3	hCD4/CD8	hCD4	hCD8
Adult	NOG	7	28.9 ± 2.9	64.1 ± 6.1	30.0 ± 4.4	14.1 ± 4.9	70.9 ± 4.2	26.5 ± 3.6	90.2 ± 12.0	62.6 ± 26.4	22.0 ± 14.9	13.1 ± 10.3
	NR2G	10	27.7 ± 13.9	69.0 ± 8.5	28.6 ± 8.8	8.2 ± 5.8	76.1 ± 8.8	22.0 ± 9.0	89.3 ± 6.2	46.9 ± 29.0	29.9 ± 17.5	15.5 ± 9.8
Newborn	NOG	6	29.5 ± 6.0	56.8 ± 8.0	35.5 ± 7.5	31.4 ± 16.0	69.5 ± 3.6	28.5 ± 3.0	88.4 ± 3.7	69.9 ± 13.2	13.9 ± 6.5	12.4 ± 5.2
	NR2G	5	24.1 ± 7.1	63.9 ± 12.9	30.5 ± 10.0	17.4 ± 5.8	70.8 ± 7.4	27.8 ± 6.7	78.8 ± 15.0	83.1 ± 6.0	10.8 ± 3.5	4.4 ± 1.7

Human cells in spleen, thymus and peripheral blood from mice at 20 weeks after HSC transplnatation were analyzed by flow cytometry.

Pearson *et al.* [12] also reported that NR1G mice showed high human cell engraftment and differentiation after HSC transplantation, similar to that in NSG mice. In the current study, we also compared the degree of human cell engraftment and differentiation among NR2G, NOG, and NOD-*scid* mice. To eliminate the influence of different sources of $CD34^+$ cells and different inoculation periods on the results of this comparison, we used the same lot of commercially available $CD34^+$ cells and inoculated them into the mice on the same day. Particularly, for the comparison between adults and newborns at the transplanted age, we obtained the newborns by Cesarean section after transplantation of their embryos from *in vitro* insemination. High engraftment of human cells from HSCs was observed in both NOG and NR2G mice regardless of inoculation age, although the HSC population in the former was slightly higher than that in the latter during the test periods. No fundamental difference in the differentiation of human cells was observed between the two mouse strains. B cells developed earlier than T cells. Namely, B cells were dominant 8 to 12 weeks after cell transplantation, but T cells became dominant from 16 weeks after cell transplantation. By contrast, no T cells developed in NOD-*scid* mice during the test period. Immunohistochemical staining of human cells in the spleen revealed that differentiated human cells were located in the same area in both NR2G and NOG mice. These results indicate that NR2G mice can be used as an alternative to NOG mice for generating humanized mice.

Regarding the age of HSC transplantation, Traggiai *et al.* [16] reported the successful generation of humanized mice by intrahepatic inoculation of HSCs into newborn BR2G mice. Ishikawa *et al.* [5] also reported the high efficiency of human cell development by intravenous HSC inoculation into newborn NSG mice. The present study also revealed that the transplantation of HSCs into newborn mice resulted in a higher engraftment rate than transplantation into adult mice. However, the difference in the engraftment rates between the mouse strains was not marked, and the differentiation of human cells was fundamentally similar, suggesting that researchers can select the age for HSC inoculation into humanized mice according to the purpose of their research.

In conclusion, newly established NR2G mice can be used as an alternative host to NOG mice for generation of humanized adult and newborn mice by inoculation of HSCs.

Acknowledgments

This work was supported by a Grant-in-Aid for Scientific Research (S) (#18100005) from the Ministry of Education, Culture, Sports, Science and Technology (MEXT), and by a grant from Research on Emerging and Re-emerging Infectious Diseases From Ministry of Health, Labour and Welfare, Japan of Japan.

References

1. Bosma, G.C., Fried, M., Custer, R.P., Carroll, A., Gibson, D.M., and Bosma, M.J. 1988. Evidence of functional lymphocytes in some (leaky) scid mice. *J. Exp. Med.* 167: 1016–1033. [Medline] [CrossRef]
2. Brehm, M.A., Cuthbert, A., Yang, C., Miller, D.M., DiIorio, P., Laning, J., Burzenski, L., Gott, B., Foreman, O., Kavirayani, A., Herlihy, M., Rossini, A.A., Shultz, L.D., and Greiner, D.L. 2010. Parameters for establishing humanized mouse models to study human immunity: analysis of human hematopoietic stem cell engraftment in three immunodeficient strains of mice bearing the IL2rgamma(null) mutation. *Clin. Immunol.* 135: 84–98. [Medline] [CrossRef]
3. Fulop, G.M. and Phillips, R.A. 1990. The scid mutation in mice causes a general defect in DNA repair. *Nature* 347: 479–482. [Medline] [CrossRef]
4. Hiramatsu, H., Nishikomori, R., Heike, T., Ito, M., Kobayashi, K., Katamura, K., and Nakahata, T. 2003. Complete reconstitution of human lymphocytes from cord blood $CD34^+$ cells using the NOD/SCID/gammacnull mice model. *Blood* 102: 873–880. [Medline] [CrossRef]
5. Ishikawa, F., Yasukawa, M., Lyons, B., Yoshida, S., Miyamoto, T., Yoshimoto, G., Watanabe, T., Akashi, K., Shultz, L.D., and Harada, M. 2005. Development of functional human blood and immune systems in NOD/SCID/IL2 receptor gamma chain(null) mice. *Blood* 106: 1565–1573. [Medline] [CrossRef]
6. Ito, M., Hiramatsu, H., Kobayashi, K., Suzue, K., Kawahata, M., Hioki, K., Ueyama, Y., Koyanagi, Y., Sugamura, K., Tsuji, K., Heike, T., and Nakahata, T. 2002. NOD/SCID/gamma(c)(null) mouse: an excellent recipient mouse model for engraftment of human cells. *Blood* 100: 3175–3182. [Medline] [CrossRef]
7. Ivanov, I.I., Atarashi, K., Manel, N., Brodie, E.L., Shima, T., Karaoz, U., Wei, D., Goldfarb, K.C., Santee, C.A., Lynch, S.V., Tanoue, T., Imaoka, A., Itoh, K., Takeda, K., Umesaki, Y., Honda, K., and Littman, D.R. 2009. Induction of intestinal Th17 cells by segmented filamentous bacteria. *Cell* 139: 485–498. [Medline] [CrossRef]
8. Lepus, C.M., Gibson, T.F., Gerber, S.A., Kawikova, I., Szczepanik, M., Hossain, J., Ablamunits, V., Kirkiles-Smith, N., Herold, K.C., Donis, R.O., Bothwell, A.L., Pober, J.S., and Harding, M.J. 2009. Comparison of human fetal liver, umbilical cord blood, and adult blood hematopoietic stem cell engraftment in NOD-scid/gammac-/-, Balb/c-Rag1-/-gammac-/-, and C.B-17-scid/bg immunodeficient mice. *Hum.*

Immunol. 70: 790–802. [Medline] [CrossRef]
9. Mombaerts, P., Iacomini, J., Johnson, R.S., Herrup, K., Tonegawa, S., and Papaioannou, V.E. 1992. RAG-1-deficient mice have no mature B and T lymphocytes. *Cell* 68: 869–877. [Medline] [CrossRef]
10. Oettinger, M.A., Stanger, B., Schatz, D.G., Glaser, T., Call, K., Housman, D., and Baltimore, D. 1992. The recombination activating genes, RAG 1 and RAG 2, are on chromosome 11p in humans and chromosome 2p in mice. *Immunogenetics* 35: 97–101. [Medline] [CrossRef]
11. Onoue, M. 1960. Studies on the radiosensitivities of four inbred strains of mice. *Jpn. J. Radiol.* 19: 2366–2370.
12. Pearson, T., Shultz, L.D., Miller, D., King, M., Laning, J., Fodor, W., Cuthbert, A., Burzenski, L., Gott, B., Lyons, B., Foreman, O., Rossini, A.A., and Greiner, D.L. 2008. Non-obese diabetic-recombination activating gene-1 (NOD-Rag1 null) interleukin (IL)-2 receptor common gamma chain (IL2r gamma null) null mice: a radioresistant model for human lymphohaematopoietic engraftment. *Clin. Exp. Immunol.* 154: 270–284. [Medline] [CrossRef]
13. Shinkai, Y., Rathbun, G., Lam, K.P., Oltz, E.M., Stewart, V., Mendelsohn, M., Charron, J., Datta, M., Young, F., Stall, A.M., *et al.* 1992. RAG-2-deficient mice lack mature lymphocytes owing to inability to initiate V(D)J rearrangement. *Cell* 68: 855–867. [Medline] [CrossRef]
14. Shultz, L.D., Lyons, B.L., Burzenski, L.M., Gott, B., Chen, X., Chaleff, S., Kotb, M., Gillies, S.D., King, M., Mangada, J., Greiner, D.L., and Handgretinger, R. 2005. Human lymphoid and myeloid cell development in NOD/LtSz-scid IL2R gamma null mice engrafted with mobilized human hemopoietic stem cells. *J. Immunol.* 174: 6477–6489. [Medline] [CrossRef]
15. Suemizu, H., Yagihashi, C., Mizushima, T., Ogura, T., Etoh, T., Kawai, K., and Ito, M. 2008. Establishing EGFP congenic mice in a NOD/Shi-scid IL2Rg(null) (NOG) genetic background using a marker-assisted selection protocol (MASP). *Exp. Anim.* 57: 471–477. [Medline] [CrossRef]
16. Traggiai, E., Chicha, L., Mazzucchelli, L., Bronz, L., Piffaretti, J.C., Lanzavecchia, A., and Manz, M.G. 2004. Development of a human adaptive immune system in cord blood cell-transplanted mice. *Science* 304: 104–107. [Medline] [CrossRef]
17. Ueda, T., Tsuji, K., Yoshino, H., Ebihara, Y., Yagasaki, H., Hisakawa, H., Mitsui, T., Manabe, A., Tanaka, R., Kobayashi, K., Ito, M., Yasukawa, K., and Nakahata, T. 2000. Expansion of human NOD/SCID-repopulating cells by stem cell factor, Flk2/Flt3 ligand, thrombopoietin, IL-6, and soluble IL-6 receptor [In Process Citation]. *J. Clin. Invest.* 105: 1013–1021. [Medline] [CrossRef]
18. Zhang, B., Duan, Z., and Zhao, Y. 2009. Mouse models with human immunity and their application in biomedical research. *J. Cell. Mol. Med.* 13: 1043–1058. [Medline] [CrossRef]

Exp. Anim. 63(1), 55–62, 2014

—Original—

A Novel Enhanced Green Fluorescent Protein-Expressing NOG Mouse for Analyzing the Microenvironment of Xenograft Tissues

Yuichiro HIGUCHI[1)], Kenji KAWAI[2)], Masafumi YAMAMOTO[1)], Miyuki KURONUMA[1)], Yasuhiko ANDO[1)], Ikumi KATANO[3)], Masato NAKAMURA[2,4)], and Hiroshi SUEMIZU[1)]

[1)]*Biomedical Research Department, Central Institute for Experimental Animals, 3–25–12 Tonomachi, Kawasaki-ku, Kawasaki, Kanagawa 210-0821, Japan*
[2)]*Pathology Department, Central Institute for Experimental Animals, 3–25–12 Tonomachi, Kawasaki-ku, Kawasaki, Kanagawa 210-0821, Japan*
[3)]*Laboratory Animal Research Department, Central Institute for Experimental Animals, 3–25–12 Tonomachi, Kawasaki-ku, Kawasaki, Kanagawa 210-0821, Japan*
[4)]*Department of Pathology and Regenerative Medicine, Tokai University School of Medicine, 143 Shimokasuya, Isehara, Kanagawa 259-1193, Japan*

Abstract: The interaction between transplanted cells and host tissues is important for the growth and maintenance of transplanted cells. To analyze the mechanisms of these interactions, a systemic fluorescent protein-expressing mouse is a useful recipient. In this study, we generated a novel NOG strain, which strongly expresses enhanced green fluorescent protein (EGFP; PgkEGFP-NOG), especially in the liver, kidney, gastrointestinal tract, and testis. Because the host tissues expressed EGFP, xenotransplanted human cancer cells were clearly identified as EGFP-negative colonies in PgkEGFP-NOG mice. Immunohistochemical analysis revealed that EGFP-expressing stromal tissues formed a complicated tumor microenvironment within xenograft tissues. Moreover, a similar microenvironment was observed in human iPS cell-derived teratomas. Collectively, these results indicated that a suitable microenvironment is essential for the growth and maintenance of xenotransplanted cells and that PgkEGFP-NOG mice represent a useful animal model for analyzing the mechanisms of microenvironment formation.

Key words: NOG mouse, teratoma, tumor microenvironment, xenotransplantation

Introduction

Cell transplantation analysis is performed for safety testing (tumorigenicity), *in vivo* functional characterization of engrafted cells, and establishment of a "humanized" mouse model [5, 10, 16, 17]. Growth and progression of transplanted cells are dependent on the formation of a suitable microenvironment [1–4, 14, 21]. For example, host stromal tissue components, such as vessels and fibroblasts, interact with engraftment derivatives and provide oxygen and other essential nutrients. To elucidate the mechanisms that form such microenvironments, various fluorescent protein-expressing murine models have been established [20, 22, 23] by mating systemically florescent protein-expressing mice with nude mice, which lack T cell production because of thymic deficiency, but retain production of B cells and other immunocompetent cells. The survivability of transplanted cells is dependent on the immune status of the recipient. It was previously demonstrated that nude mice showed

(Received 13 June 2013 / Accepted 22 July 2013)
Address corresponding: Y. Higuchi, Biomedical Research Department, Central Institute for Experimental Animals, 3–25–12 Tonomachi, Kawasaki-ku, Kawasaki, Kanagawa, 210-0821, Japan

a little resistance to xenotransplantation [10]. Another group reported the nonobese diabetic/severe combined immunodeficient (NOD/Scid) transgenic mouse expressing enhanced green fluorescent protein (EGFP) [11]. NOD/Scid mice lack B and T lymphocytes and have low natural killer (NK) cells and hemolytic complement activity, defects in myeloid development, and poor antigen-presenting-cell function. The NOD/Scid mouse demonstrates immunodeficiency that is severer than that in the nude mouse. However, it was reported that lymphoma developed in the NOD/Scid mouse with high incidence [7].

We previously established a nonobese diabetic/severe combined immunodeficiency interleukin-2 receptor γ^{null}(NOD/Shi-*scid* *Il2rg*^{null}) (NOG) mouse that incorporated the *Il2rg*^{null} mutation from C57BL/6-*Il2rg*^{tmlSug} mice by backcross mating with NOD/Shi-*scid* mice [6]. NOG mice have no lymphocytes or NK cells and have impaired dendritic cells and macrophage function [9, 13]. Additionally, we previously reported an EGFP-expressing NOG mouse line (NOG-EGFP mouse) [18]. Since the NOG-EGFP mouse demonstrates severe immunodeficiency and systemic EGFP expression, it is considered the most appropriate recipient mouse for analyzing the microenvironment of xenograft tissues [15].

The NOG-EGFP mouse demonstrated strong EGFP expression especially in the skin, muscle, and pancreas. However, EGFP expression in the hepatic parenchymal cells was not observed (Fig. S1). This suggests that the NOG-EGFP mouse is not suitable as a recipient for liver metastatic model. In the present study, we established a novel EGFP-expressing NOG mouse that expressed EGFP under the control of the phosphoglycerate kinase promoter (PgkEGFP-NOG mouse). The PgkEGFP-NOG mouse retains equivalent immunodeficiency to the NOG mouse, and whole-body immunohistochemical analysis revealed that PgkEGFP-NOG mice demonstrated strong EGFP expression especially in the liver. Xenograft colonies in the PgkEGFP-NOG mice were clearly identified as EGFP-negative colonies, and the tumor microenvironment in xenograft colonies was composed of EGFP-expressing fibroblasts and vessels. Moreover, a similar microenvironment was observed in human induced pluripotent stem (iPS) cell-derived teratomas. These results demonstrated that PgkEGFP-NOG mice present a useful host model for analysis of the microenvironment of xenograft tissues.

Materials and Methods

DNA construction

The *EGFP* gene expression unit was constructed as follows. The promoter region (621 bp) of the murine phosphoglycerate kinase 1 gene was amplified by polymerase chain reaction (PCR) at an annealing temperature of 60°C with the primers mPGK-F-*Ase*I (5′-AAAATTAATACCGGGTAGGGGAGGCGCT-3′) and mPGK-R-*Bam*HI (5′-TTTGGATCCACGCGCTTCTACAAGGCGCT-3′) and then cloned into the pEGFP-N1 plasmid (Clontech Laboratories, Inc., Mountain View, CA, USA) at the *Ase* I-*Bam* HI restriction site (pmPgkEGFP). A vector-free 1.6-kb *EGFP* expression fragment was prepared by cleavage of the pmPgkEGFP plasmid DNA at unique *Ase* I and *Ssp* I restriction sites.

Generation of the PgkEGFP-NOG mouse

The PgkEGFP-NOG construct was microinjected into fertilized NOD/Shi strain mouse eggs using standard methods. Transgenic offspring were identified by PCR (annealing temperature 60°C) using GFPF1 forward and reverse primers (5′-CTGGTCGAGCTGGACGGCGACG-3′ and 5′-CACGAACTCCAGCAGGACCATG-3′, respectively). Genomic DNA extracted from tail tissue was amplified in a 20 μl reaction volume under the following conditions: 94°C for 2 min; 30 cycles at 94°C for 30 s, 60°C for 30 s, and 72°C for 30 s; and a final extension step at 72°C for 3 min. Transgene DNA showed an amplified product band of 630 bp on agarose gel electrophoresis. For cloning of the transgene/transgene junction, PCR amplification was conducted using PgkEGFP-NOG mouse DNA and the GFPF1 forward primer and PGKR1 reverse primer, 5′-AGAAAGCGAAGGAGCAAAGCT-3′. Nucleotide sequences of the transgene/transgene junction were determined using an ABI PRISM 3130 × l Genetic Analyzer (Life Technologies Corporation, Carlsbad, CA, USA) and ABI PRISM BigDye Terminator Cycle Sequencing Ready Reaction Kits (Life Technologies Corporation). Transgenic females were mated with NOG males to confer the *scid* and *Il2rg*^{null} mutations to the offspring. The *Il2rg*^{null} mutations were genotyped using a previously described PCR method [6]. The *scid* mutations were genotyped using Cycling Probe Technology (Cycleave®PCR Reaction Mix, Takara Bio Inc., Shiga, Japan). Information for the primers and probes is provided in the supplementary table. Reaction mixture composition and cycling conditions were in

accordance with the instruction manual. Real-time PCR was performed using an Applied Biosystems 7500 Fast Real-Time PCR System, and data were collected using the SDS 2.6 application software (ABI). EGFP expression in the PgkEGFP-NOG mouse was then confirmed with the IVIS Spectrum CT and Living Image software (Perkin Elmer Inc., Waltham, MA, USA). For flow cytometric analysis of peripheral blood, hemolysis was performed as previously described [6]. Samples were analyzed using a FACSCanto analyzer (BD). Data were recorded with the BD FACSDiva Software (BD) and analyzed using the FlowJo software (Tree Star). The murine line used in the present study was assigned the genetic designation NOG-*Tg (Pgk-EGFP) 16*/ShiJic (formally, NOD.Cg-*Prkdc*^{scid} *Il2rg*^{tm1Sug} *Tg (Pgk-EGFP) 16*/ShiJic, abridged name: PgkEGFP-NOG). We also generated BALB/cA.Cg-*Tg (Pgk-EGFP) 16*/Jic (abridged name, PgkEGFP-BALB) and C57BL/6J.Cg-*Tg (Pgk-EGFP) 16*/Jic (abridged name, PgkEGFP-C57BL/6) by crossing the inbred PgkEGFP-NOG strain with the BALB/cA or C57BL/6J strain, respectively, using the speed congenic method [18]. This study was performed in accordance with the guidelines of our institution and was approved by the Animal Experimentation Committee of the Central Institute for Experimental Animals.

Cell culture

The human colorectal cancer cell line HCT 116 was obtained from the American Type Culture Collection (Manassas, VA, USA). HCT 116 cells were maintained in Dulbecco's Modified Eagle Medium (DMEM; Invitrogen Corporation, Carlsbad, CA, USA) supplemented with 10% fetal bovine serum (Invitrogen), 2 mM L-glutamine (L-Gln; Nacalai Tesque, Inc., Kyoto, Japan), 50 units/ml of penicillin, and 50 μg/ml of streptomycin (P–S; Nacalai Tesque, Inc.).

Human iPS cell line 201B7 was provided by the RIKEN BRC (Ibaraki, Japan) through the National Bio-Resource Project of the Ministry of Education, Culture, Sports, Science and Technology (MEXT), Japan [19]. Human iPS cells were maintained with mitomycin C-treated mouse embryonic fibroblast feeder cells in DMEM:Nutrient Mixture F-12 (Invitrogen) supplemented with 20% knockout serum replacement (KSR; Invitrogen), L-Gln, P–S, 100 μM nonessential amino acids (Invitrogen), 100 μM β-mercaptoethanol (Sigma-Aldrich, St. Louis, MO, USA), and 5 ng/ml of basic fibroblast growth factor (Wako Pure Chemical Industries, Ltd., Osaka, Japan).

Transplantation

Confluent HCT 116 cells were dissociated using 0.25% trypsin- ethylenediaminetetraacetic acid (EDTA; Invitrogen). For subcutaneous transplantation, 1×10^5 HCT 116 cells were suspended in 100 μl of Hanks' Balanced Salt Solution (HBSS, Invitrogen) and subcutaneously injected. For transplantation under the kidney capsule, the kidney was exteriorized through a dorsal-horizontal incision, and a syringe with a 29-G needle with a flattened tip was introduced into the kidney at a site away from the transplanted region. The kidney was penetrated, the tip of the needle was held just beneath the kidney capsule, and 1×10^4 HCT 116 cells in 10 μl of HBSS were injected. For transplantation into the testis, 1×10^4 HCT 116 cells in 10 μl of HBSS were injected into the testis using a syringe with a 29-G needle. In the case of intrasplenic (isp) injection, 1×10^4 HCT 116 cells in 50 μl HBSS were injected isp using a Hamilton syringe with a 26-G needle, as previously described [8]. Recovered grafts were embedded in optimal cutting temperature compound (Sakura Finetechnical Co., Ltd., Nagoya, Japan). Fresh frozen sections were immediately fixed with 4% paraformaldehyde (PFA) or 100% ethanol. For the observation of EGFP fluorescence, PFA-fixed samples were embedded in ImmunoSelect Antifading Mounting Medium (Dianova, Inc., Pinole, CA, USA) and then analyzed by fluorescent microscopy (Carl Zeiss Microscopy GmbH, Jena, Germany).

To assess teratoma formation, confluent human iPS cells were treated with phosphate-buffered saline (Nacalai Tesque, Inc.) supplemented with 20% KSR, 0.25% trypsin (Invitrogen), 1 mg/ml of collagenase IV (Invitrogen) and 10 mM $CaCl_2$ (Nacalai Tesque, Inc.) for 5 min. Cell clusters were gently detached using a cell scraper and collected in a 15-ml conical tube. A part of the cell suspension was treated with 0.25% trypsin-EDTA and used for cell counting. Next, 1×10^7 human iPS cells were suspended in 0.2 ml of HBSS and then subcutaneously injected into the mice. Eight weeks post-transplantation, the teratomas were recovered and fixed with 10 nM Mildform formaldehyde solution (Wako Pure Chemical Industries, Ltd.). Paraffin-embedded tissues were then sliced and stained with hematoxylin and eosin (HE).

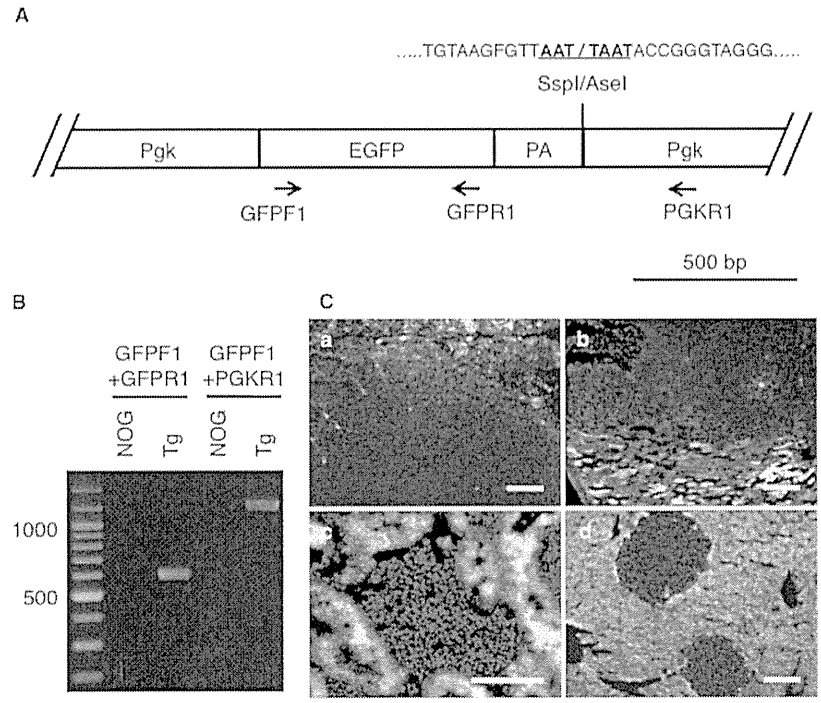

Fig. 1. Establishment of the PgkEGFP-NOG mouse. A. A schematic representation of the inserted transgenes. The GFPF1+GFPR1 primer set was used for genotyping PCR, and the GFPF1+PGKR1 primer set was used to sequence the tandem transgene junction. The nucleotide sequence of the tandem transgene junction was described. B. The PCR products of the primer sets GFPF1+GFPR1 (630 bp) and GFPF1+PGKR1 (1288 bp). NOG mice were used as negative controls (Non). Tg indicates the PgkEGFP-NOG offspring. C. HCT 116 cells were transplanted into subcutaneous (a), kidney (b), testis (c), and liver tissues (d) of the PgkEGFP-NOG mice. Xenotransplanted organs were recovered 2 weeks after transplantation, and fresh frozen sections were analyzed by fluorescence microscopy. The green fluorescence indicates EGFP, and blue indicates nuclear staining (DAPI). Xenografts in the PgkEGFP-NOG mice were clearly identified as EGFP-negative colonies. *Bar=200 μm.

Immunohistochemical analysis

The following antibodies were used for immunohistochemical analysis: mouse anti-human leukocyte antigen (Hokudo Co., Ltd., Hokkaido, Japan), rabbit anti-vimentin (Nichirei Bioscience, Tokyo, Japan), and anti-GFP (Abcam Inc., Cambridge, MA, USA). The antibodies for mouse immunoglobulins were visualized using amino acid polymer/peroxidase complex-labeled antibodies (Histofine Simple Stain Mouse MAX PO (M); Nichirei Bioscience) and diaminobenzidine (Dojindo Laboratories, Kumamoto, Japan) substrate (0.2 mg/ml 3,3′-diaminobenzidine tetrahydrochloride, 0.05 M Tris-HCl (pH 7.6), and 0.005% H_2O_2). Sections were counterstained with hematoxylin.

Results

Establishment of the PgkEGFP-NOG mouse line

The *PgkEGFP* transgene was microinjected into fertilized NOD/Shi strain mouse eggs and confirmed by genomic PCR, and the sequence of the tandem transgene junction was defined (Figs. 1 A and B). Transgenic offspring were mated with NOG mice, and insertion of the *scid* and *Il2rg*^{null} mutations was confirmed as previously described [6]. Next, we confirmed EGFP expression in the PgkEGFP-NOG mice (Figs. S1–S3). Although EGFP expression in the cardiac muscle, skeletal muscle and pancreatic exocrine cells was faint (Figs. S1 and S3), EGFP expression was systemically observed (including in the liver parenchymal and ductal epithelium cells). Furthermore, no sexual dimorphism was observed (data

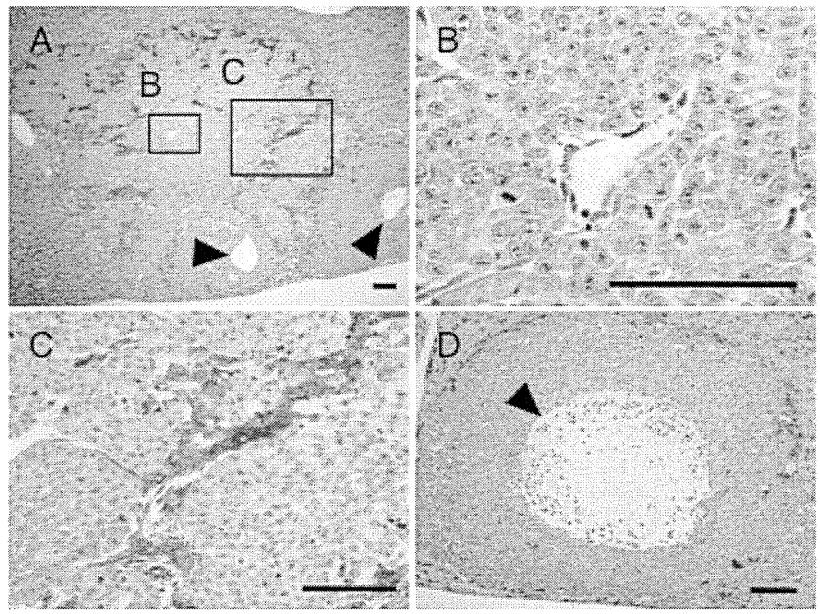

Fig. 2. Tumor microenvironment in the xenograft colonies composed of EGFP-expressing stromal tissue components. HCT 116 cells were intrasplenically transplanted into the livers of PgkEGFP-NOG mice. Xenotransplanted livers were recovered 3 weeks after transplantation, and EGFP-expressing tissues in the xenografts were subjected to immunohistochemical analysis. In the recovered livers, the xenografts were identified as EGFP-negative colonies (A). EGFP-expressing vessels (B) and fibroblasts (C) formed the tumor microenvironment in the xenograft colonies. On the other hand, EGFP-expressing stromal tissues were not observed in the necrotic areas (A and D, arrowheads). *Bar=100 μm.

not shown). Since the host tissues expressed EGFP, engraftment derivatives that were transplanted in the PgkEGFP-NOG mice appeared to be EGFP-negative. We then transplanted the human colon cancer cell line, HCT 116, into the PgkEGFP-NOG mice. HCT 116 cells were transplanted into subcutaneous, kidney capsule, testis, and liver tissues of the PgkEGFP-NOG mice, and each transplanted organ was recovered 2 weeks posttransplantation. EGFP fluorescence analysis revealed that the HCT 116-derived xenografts could be clearly distinguished from host tissues, which displayed EGFP fluorescence (Fig. 1 C). Immunohistochemical analysis of the xenografts demonstrated that EGFP-negative tissues were positively counterstained with human leukocyte antigen (HLA; Fig. S4). Collectively, these results indicated that the xenografts in the PgkEGFP-NOG mice were clearly identified by the absence of EGFP expression.

Tumor microenvironment analysis in PgkEGFP-NOG mice

To investigate the tumor microenvironment, we performed isp transplantation of the HCT 116 cells into PgkEGFP-NOG mice. The xenotransplanted livers were recovered 3 weeks after transplantation and subjected to immunohistochemical analysis. EGFP-expressing stromal tissue components (i.e., vessels and fibroblasts) were readily identified in the xenograft tissues and formed a complicated tumor microenvironment (Figs. 2 A–C). We also observed necrotic areas in the xenografts (Figs. 2 A and D). In accordance with a previous report, EGFP-expressing vessels and fibroblasts were not observed in the necrotic areas [22]. Collectively, these results indicated that the interaction between the xenograft and host tissues is important for tumor growth and maintenance. Next, we examined teratoma formation in the subcutaneously injected PgkEGFP-NOG mice. It is well known that human iPS cells can differentiate into stromal tissue components. However, EGFP-expressing vascular cells and fibroblasts were clearly distinguishable from xenotransplanted derivatives (Figs. 3 B and E). The microenvironment was composed of EGFP-expressing tissues and human iPS cell derivatives, which stained posi-